A Heteroclinic Connection between two Saddle Slow Manifolds in the Olsen Model

Elle Musoke, Bernd Krauskopf and Hinke M. Osinga
Department of Mathematics, University of Auckland, Private Bag 92019
Auckland, 1142, New Zealand
elle.musoke@auckland.ac.nz

The abstract should summarise the context, content and conclusions of the paper. It should not contain any references or displayed equations. Typeset the abstract in 10 pt Times Roman with baselineskip of 12 pt, making an indentation of 1.6 cm on the left and right margins.

Keywords: A list of 3–5 keywords are to be supplied.

1. Introduction

Slow-fast dynamical systems are characterized by a separation of variables into those that evolve on a fast time scale and those that evolve on a slower time scale. The separation of variables into fast and slow can be found in many systems in the world around us: chemical systems, neurons, electric circuits, lasers and predator-prey dynamics have been, among others, described by slow-fast models [Brøens & Bar-Eli, 1991; De Maesschalck & Wechselberger, 2015; van der Pol, 1927; Otto *et al.*, 2012; Piltz *et al.*, 2017]. By reason of their ubiquity, the various phenomena that arise from the multiple-time-scale nature of slow-fast systems are of significant interest. These have been be described for two- and three-dimensional systems by well-established theory [Benoît *et al.*, 1981; Benoît, 1982, 1985; Guckenheimer, 1985; Brøens *et al.*, 2006; Krupa *et al.*, 2008]. Small-amplitude limit cycles transitioning to larger-amplitude relaxation oscillations were studied in two dimensions, for example, the Van der Pol oscillator and Fitz-Hugh-Nagumo model [Benoît *et al.*, 1981; FitzHugh, 1955]. In three-dimensional systems, periodic orbits with epochs of localized small-amplitude oscillations (SAOs) and epochs of large-amplitude oscillations (LAOs) have been observed [Hudson *et al.*, 1979]. The mechanisms that cause SAOs of these appropriately named mixed-mode oscillations (MMOs) are described in [Desroches *et al.*, 2012]. We now investigate novel phenomena that arise in four-dimensional slow-fast systems which may provide insight into undiscovered mechanisms for MMOs.

We consider a prototypical four-dimensional slow-fast dynamical system which exhibits MMOs. We study the so-called Olsen model for peroxidase-oxidase reaction, first introduced by Lars F. Olsen in 1983 [Olsen, 1983], in a parameter regime corresponding to three fast and one slow variable. Mechanisms for MMOs in the Olsen model were previously investigated in [Desroches *et al.*, 2009] after an assumption was made to reduce the model to a three-dimensional system. Manifolds on which the flow progresses on the slower timescale were computed along with the manifolds consisting of trajectories that converged to them in forward and backwards time respectively. These were found to be very insightful into the formation of MMOs as well as the cause of their particular geometry. However, because of the assumptions

Table 1.   System parameters for system (1)

α	δ	ε	η	κ	μ	ζ
0.0912	1.2121e-04	0.0037	0.0540	3.7963	0.9697	0.9847

used to reduce the model to a three-dimensional system, some of the computed manifolds were found to be of lower dimension than the corresponding manifolds in the full system. In this research, we develop techniques for computing the same manifolds in the full four-dimensional model in the interest of studying their geometry and interactions with each other. In particular, we focus on interactions between higher-dimensional manifolds that do not exist in systems of three dimensions or lower.

To better observe the separation between fast and slow variables, we use a change of coordinates described in [Kuehn & Szmolyan, 2015] and given by the system of ODEs

$$\begin{cases} \frac{dA}{dt} & = \mu - \alpha A - ABY, \\ \frac{dB}{dt} & = \varepsilon(1 - BX - ABY), \\ \frac{dX}{dt} & = \frac{1}{\eta}(BX - X^2 + 3ABY - \zeta X + \delta), \\ \frac{dY}{dt} & = \frac{\kappa}{\eta}(X^2 - Y - ABY), \end{cases} \quad (1)$$

where $(A, B, X, Y) \in \mathbb{R}^4$ are positive concentrations of chemicals. The system parameters given by Greek letters in Table 1 are functions of original system parameters given in [Olsen, 1983]. They were chosen to be the same as in [Kuehn & Szmolyan, 2015] with a minor modification. Note that for notational convenience, we have substituted ε_b and ε^2 [Kuehn & Szmolyan, 2015] with ε and η respectively.

The classification of variables as either slow or fast is not straightforward for the Olsen model because the variables are not consistently slow or fast over all regions of phase space. In fact system (1) nominally has three different time scales. The time-scaling parameters ε and η depend on the original system parameter k_1. As suggested by [Kuehn & Szmolyan, 2015], we decrease k_1 past 0.16 to 0.1 so that there are only two time scales. We study a parameter regime corresponding to three fast variables, A, X and Y, and one slow variable, B.

2. Background

In the limit as $\varepsilon \to 0$, system (1) becomes

$$\begin{cases} \frac{dA}{dt} & = \mu - \alpha A - ABY, \\ \frac{dX}{dt} & = \frac{1}{\eta}(BX - X^2 + 3ABY - \zeta X + \delta), \\ \frac{dY}{dt} & = \frac{\kappa}{\eta}(X^2 - Y - ABY), \end{cases} \quad (2)$$

in which B is a parameter. We refer to the three-dimensional system (2) as the layer equation or the fast subsystem. If one first performs a time rescaling, $\tau = \varepsilon t$, and then considers the limit as $\varepsilon \to 0$ the system reduces to

$$\begin{cases} 0 & = \mu - \alpha A - ABY, \\ \frac{dB}{d\tau} & = (1 - BX - ABY), \\ 0 & = \frac{1}{\eta}(BX - X^2 + 3ABY - \zeta X + \delta), \\ 0 & = \frac{\kappa}{\eta}(X^2 - Y - ABY), \end{cases} \quad (3)$$

which is a differential algebraic system called the slow subsystem or the reduced system. The three algebraic equations in system (3) define a one-dimensional manifold called the critical manifold, C. The flow in (3) is defined by the single differential equation for B and it is confined to C.
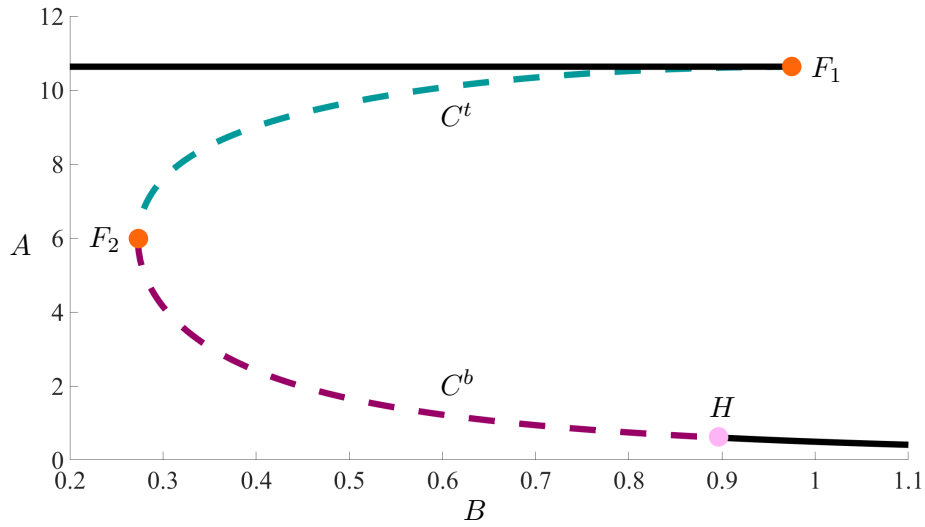
Fig. 1.   Physically relevant branches of the critical manifold of system (1) shown in projection onto the (B,A)-plane. The branches labeled C^t and C^b and colored teal correspond to saddle equilibria of (2), solid curves indicate stable nodes. The two saddle-node bifurcations are represented as orange dots and labeled F_1 and F_2 respectively. The Hopf bifurcation is represented with a light pink dot and is labeled H.

The critical manifold consists of equilibria of the fast subsystem for different values of B. These can be linearized about and their stability determined by the 3×3 Jacobian matrix of (2). Equilibria at which the Jacobian's eigenvalues all have non-zero real parts are called hyperbolic, otherwise we say that the equilibrium is non-hyperbolic. Non-hyperbolic equilibria lying on the critical manifold correspond to local bifurcations in (2). The critical manifold has 11 branches near a stable MMO of interest, separated from each other by non-hyperbolic equilibria of the fast subsystem.

Figure 1 shows four branches of C on which all variables are positive projected into the (B,A)-plane. Seven nearby branches of C are not shown, because they lie in regions where at least one of A, B, X, or Y is negative and not physically relevant. Of the branches shown in Figure 1, the topmost black branch consists of stable equilibria of (2) and is separated from the teal colored branch of saddle equilibria, denoted C^t, by a fold, shown in orange and denoted F_1, occurring at $B \approx 0.956$. Equilibria $p \in C^t$ each have a two-dimensional linear stable space $E^s(p)$ and a one-dimensional linear unstable space $E^u(p)$. The flow is from left to right near C^t in the (B, A)-projection shown. The fold F_1 has the appearance of a cusp in the (B,A)-projection, however (B,X)- and (B,Y)- projections show that this is truly a fold with respect to B. Another fold, also shown in orange, separates C^t from a lower raspberry colored branch of saddle equilibria and occurs at $B \approx 0.273$ and is denoted F_2. The raspberry branch of saddle equilibria is denoted C^b and is separated from a branch of stable equilibria on the right by a Hopf bifurcation, represented as a pink dot and denoted H, occurring at $B \approx 0.896$. Equilibria on C^b have each one stable and two unstable eigenvectors. The flow is from right to left near C^b.

We denote the local stable and unstable manifolds of points $p \in C$ by $W^s_{loc}(p)$ and $W^u_{loc}(p)$. These are the trajectories in 2 that converge to p in forwards and backwards time respectively. The saddle branch C^t has a three-dimensional local stable manifold $W^s_{loc}(C^t)$ and a two-dimensional local unstable manifold $W^u_{loc}(C^t)$ defined as

$$W^s_{loc}(C^t) = \bigcup_{p \in C^t} W^s_{loc}(p), \qquad W^u_{loc}(C^t) = \bigcup_{p \in C^t} W^u_{loc}(p).$$

Similarly C^b has a three-dimensional local unstable manifold and a two-dimensional local stable manifold defined as

$$W_{loc}^s(C^b) = \bigcup_{p \in C^b} W_{loc}^s(p), \qquad W_{loc}^u(C^b) = \bigcup_{p \in C^b} W_{loc}^u(p).$$

We are interested in interactions between stable and unstable manifolds of C^t and C^b as $\varepsilon > 0$. Although the branches C^t and C^b of the critical manifold are no longer invariant for $\varepsilon > 0$, Fenichel Theory guarantees that both C^t and C^b persist as locally-invariant manifolds called slow manifolds, denoted S^t and S^b, that are not unique [Fenichel, 1979]. Orbit segments that lie on a slow manifold remain slow for an $O(1)$ amount of slow timescale time. Locally invariant means that solutions can only enter or leave the manifold via its edges.

We can select a unique representative S^t by considering the slow manifold that remains slow for the longest amount of time. The slow manifold S^t has the same dimension as C^t and, as $\varepsilon \to 0$, orbit segments converge to C^t. Since equilibria of (2) lying on C^t are of saddle type, C^t and S^t are also of saddle type. The slow manifold, S^b, associated with C^b can be similarly defined.

Fenichel Theory also guarantees that $W_{loc}^s(C^t)$ and $W_{loc}^u(C^t)$ persist as locally-invariant local stable and unstable manifolds of S^t [Fenichel, 1979]. We define the stable manifold of S^t as a family of orbit segments, W^s, that have a fast approach to S^t and then stay close to it for an $O(1)$ amount of time. Similarly, we define the unstable manifold as a family of orbit segments, W^s, that approach S^t in backward time and then stay close to it for an $O(1)$ amount of backward time. According to Fenichel Theory, W^s and W^u have the same dimensions as $W_{loc}^s(C^t)$ and $W_{loc}^u(C^t)$ and lie at an $O(\varepsilon)$ distance away from them, respectively. The manifolds W^s and W^u are not unique, however they can be made unique by imposing additional conditions. We can similarly define the stable and unstable manifolds associated with C^b, denoted $W^s(S^b)$ and $W^u(S^b)$, respectively.

3. Computation of One-Dimensional Saddle Slow Manifolds

For the computation of a one-dimensional saddle slow manifold, we follow the presentation in [Farjami *et al.*, 2018] of a one-dimensional saddle slow manifold for a three-dimensional system. Here we consider only the slow manifold S^t associated with C^t; the slow manifold S^b can be found in a similar manner.

The precise definition of the slow manifold S^t is given with respect to a closed interval $[B_{in}^t, B_{out}^t]$ for the slow variable B. The values for B_{in}^t and B_{out}^t are chosen such that the interval is contained in the interval defined by the B-coordinates of the two fold points F_1 and F_2. Note that there is a segment in C^t for which each point $p \in C^t$ is uniquely associated via its B-coordinate with a value for $B_p \in [B_{in}^t, B_{out}^t]$. For each $B_p \in [B_{in}^t, B_{out}^t]$ there is a unique point $p = (p_A, p_B, p_X, p_Y) \in C^t$ such that $p_B = B_p$. We define a solid three-sphere $D_\delta(B_p)$ in the three-dimensional subsection $B = p_B$ that has radius δ and center p, given formally by

$$D_\delta(B_p) = \{w \in \mathbb{R}^4 | w_B = B, |w - p| \le \delta\}.$$

The union $\mathscr{D} = \cup_{B \in [B_{in}^t, B_{out}^t]} D_\delta(B)$ forms a four-dimensional compact cylinder. The radius δ is small, but it needs to be at least of $O(\varepsilon)$ to ensure that S^t lies in $\mathscr{D}$. The one-parameter family of orbit segments that enter $\mathscr{D}$ via $D_\delta(B_{in}^t)$ and exit via $D_\delta(B_{out}^t)$ are candidates for S^t. We impose the additional condition that S^t must have maximal integration time in $\mathscr{D}$ to select a unique candidate to represent S^t. This condition may be interpreted as selecting S^t such that it enters $\mathscr{D}$ via W^s and exits via W^u.

The set-up is similar to the set-up described in [Farjami *et al.*, 2018] with the difference that $D_\delta(B_{in}^t)$ and $D_\delta(B_{out}^t)$ are three-spheres rather than two-dimensional disks and $\mathscr{D}$ is four dimensional rather than three dimensional. Plotted in green in Figure 2 is a projection of the unique representative of S^t. Sketched in purple is $\mathscr{D}$ with the spheres $D_\delta(B_{in}^t)$ and $D_\delta(B_{out}^t)$ at either end.

3.1. *Boundary value implementation*

We compute S^t by setting up an appropriately defined two-point boundary-value problem (2PBVP) with the pseudo-arclength continuation package Auto [Doedel, 2007]. We view S^t as an orbit segment $\mathbf{u} =$
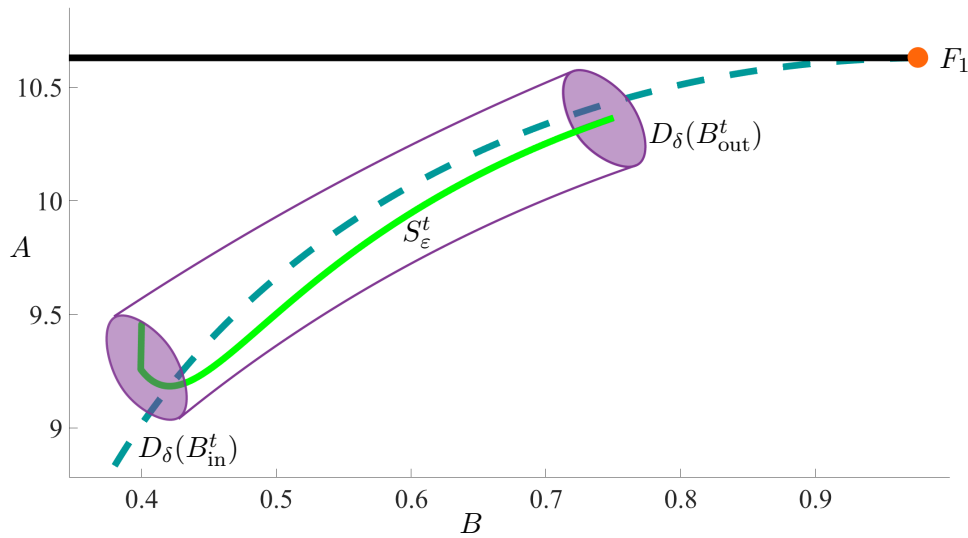
Fig. 2.   A visualization of the slow manifold definition projected into the (B, A)-plane. The spheres $D_\delta(B_{in}^t)$ and $D_\delta(B_{out}^t)$ are represented by purple disks at either end of a four-dimensional cylinder, also represented in purple. A computation of the slow manifold is plotted in green and labelled S^t.

$\{\mathbf{u}(s) | 0 \le s \le 1\}$ of the rescaled system

$$\frac{d\mathbf{u}}{ds} = TF(\mathbf{u}), \tag{4}$$

where $\mathbf{u}(s) = (A(s), B(s), X(s), Y(s)) \in \mathbb{R}^4$ is the vector of chemical concentrations, F is the right-hand side of (1) and T is the total integration time on the fast timescale, $t = Ts$.

To obtain an initial solution of (4), we perform a homotopy step as follows. First, we choose $B_{out}^t = 0.75$ at a value that corresponds to a point $p_{out}^t \in C^t$ close to F_1. We then impose the conditions

$$\mathbf{u}(0) \in E^u(C^t), \tag{5}$$

and

$$\mathbf{u}(1) \in E^s(p_{out}^t), \tag{6}$$

that each impose two conditions on $\mathbf{u}(0)$ and $\mathbf{u}(1)$, respectively. The point p is then a solution to the two-point boundary-value problem defined by (4)–(6) with $T = 0$. We then decrease $\mathbf{u}_B(0)$ towards $S1$ while the total integration time increases. The integration is stopped when $\mathbf{u}_B(0) = 0.4$, corresponding to the point $p^* \in C^t$, before it reaches F_2.

We remark that $D_\delta(B_{in}^t)$ defines a three-parameter family of orbit segments with initial conditions in the sphere. We can refine our search for orbits that enter the cylinder via $D_\delta(B_{in}^t)$ and exit it via $D_\delta(B_{out}^t)$ by observing that, because S^t is of saddle type, the initial point of a candidate orbit segment must lie in a small neighborhood of W^s in the sphere $D_\delta(B_{in}^t)$. Similarly the end point must remain in a small neighborhood of W^u in the sphere $D_\delta(B_{out}^t)$.

We define the two-dimensional plane $\Phi = \{E^u(p_{in}^t) + \begin{bmatrix} 0 & 0 & 0 & Y \end{bmatrix}^T | Y \in \mathbb{R}\}$ that is transverse to $W^s \cap D_\delta(B_{in}^t)$ and contains $E^u(p^*)$. We impose the boundary conditions

$$\mathbf{u}(0) \in \Phi \tag{7}$$

which also imposes two conditions on $\mathbf{u}(0)$. The orbit segment resulting from the homotopy step is then a solution to the 2PBVP defined by (4), 6, and (7). The total integration time T is a free parameter in

this 2PBVP, which means that there exists a one-parameter family of solutions. To select a unique orbit segment from this solution family, we impose the additional condition that T be locally maximal. This will be the orbit segment which locally has the longest slow segment in the geometric sense and will be the best approximation of S^t. In the case where there are two such candidates, we choose one.

In the final continuation run we increase the integration time until a fold in T is detected. The resulting orbit segment approximates the saddle slow manifold, S^t.

A projection of S^t into the (B, A)-plane is shown as the green curve in Figure 2. A keen observer will note that, near $D_\delta(B_{\rm in}^t)$, S^t includes a segment of sharp decrease mostly in the A-direction. This is due to the final step in our computation, where we restrict $\mathbf{u}(0)$ to move in the plane Σ. In order to increase the integration time, $\mathbf{u}(0)$ then moves toward the intersection of W^s with Σ while $\mathbf{u}(1)$ moves toward the intersection of $E^s(p_{\rm out}^t)$ with W^u. The fold in T signals when $u(0)$ and $u(1)$ are near respective intersection points and the result is an orbit segment containing fast segments lying on W^s and W^u. In Figure 2, the segment lying on W^u is so short that it is not visible. We obtain an approximation of S^t that does not include fast segments by restricting the orbit segment further within the interval $[B_{\rm in}^t, B_{\rm out}^t]$.

An approximation of the slow manifold associated with C^b can be computed in the same way by choosing $B_{\rm in}^b$ near H, and $B_{\rm out}^b$ near $S2$ in the above definition. We choose $B_{\rm in}^b = B_{\rm out}^b$ smaller than and near H_B.

4.   The Stable Manifold of a Slow Manifold

Fenichel theory guarantees that each slow manifold S^t, associated with C^t, has a local, two-dimensional unstable manifold $W_{\rm loc}^u$ [Fenichel, 1979]. By definition, such an unstable manifold consists of a one-parameter family of orbit segments that have a fast approach to S^t in backward time before remaining $O(\varepsilon)$ close for $O(1)$ (backward) time. However, the unstable manifold of a saddle slow manifold is not unique and we consider only a specific candidate $W_{\rm loc}^u$ from this non-unique family of manifolds that all lie exponentially close to each other [Fenichel, 1979]. Similarly there exists a local, non-unique, three-dimensional stable manifold $W_{\rm loc}^s(S^t)$, which is defined as a two-parameter family of orbit segments that have a fast approach to S^t in forward time before remaining $O(\varepsilon)$ close for $O(1)$ time. The global unstable and stable manifolds W^u and W^s can be obtained from extending $W_{\rm loc}^u$ and $W_{\rm loc}^s$ in backward and forward time, respectively. In [Desroches *et al.*, 2009], a two-dimensional approximation of W^s was computed in the region between C^t and C^b. We now turn to the computation of the three-dimensional manifold in the full system.

As W^s is three-dimensional it is cumbersome to compute and difficult to visualize. A natural way forward is to study a subset of W^s as a one-parameter family of two-dimensional slices. These can be visualized and computed with the pseudo-arclength continuation package Auto [Doedel, 2007]. We begin by defining a two-dimensional plane Σ given by fixed values of A and either X or Y. We approximate a slice with a smooth, one-parameter family of $\mathbf{u}$ that begin in Σ, enter $\mathscr{D}$ at $D_\delta(B)$ for some $B^* \in [B_{\rm in}^t, B_{out}^t]$, and remain inside $\mathscr{D}$ for $O(1)$ time. We denote such an approximation by W_Σ^s. It is only the portions of the $\mathbf{u}$ that enter $\mathscr{D}$ in the fast direction that are considered to be part of W_Σ^s. The portions that evolve mostly in the B-direction inside $\mathscr{D}$ for $O(1)$ time are considered to be part of S^t. If a $\mathbf{u}$ includes a portion that has a fast exit from $\mathscr{D}$, that portion is considered an approximation of an orbit segment lying on W^u.

4.1.   *Boundary value problem implementation*

We are interested in the geometry of W_Σ^s in the region between C^t and C^b where W^s was found in [Desroches *et al.*, 2009]. We define the plane Σ^*, given by fixing $A \approx 10.6055$ and $Y \approx 2.3001 \times 10^{-4}$, and compute $W_{\Sigma^*}^s$ by adapting a technique outlined in [Farjami *et al.*, 2018] for two-dimensional stable manifolds in three-dimensional systems. We then explain the computation of W_Σ^s for an arbitrary Σ that is transverse to the flow and $E^s(C^t) = \bigcup_{p \in C^t} E^u(p)$ in our region of interest.

We first perform a homotopy step by choosing $B_{\rm out}^t = 0.9$ corresponding to the point $p_{\rm out}^t \approx [10.6055, 0.9, 4.9248 \times 10^{-2}, 2.3001 \times 10^{-4}]$. Following the definition for $W_{\Sigma^*}^s(S^t)$, we impose the boundary condition

$$\mathbf{u}(0) \in \Sigma^* \tag{8}$$

which imposes two conditions on $\mathbf{u}(0)$ since Σ^* is two dimensional. As part of selecting a $\mathbf{u}$ that remains close to S^t for $O(1)$ time, we consider the two-dimensional $E^s(p_{\text{out}}^t)$ that is transverse to W^u. We impose the boundary condition

$$\mathbf{u}(1) \in E^s(p_{\text{out}}^t) \tag{9}$$

which imposes two conditions on $\mathbf{u}(1)$ and allows for the possibility of $\mathbf{u}(1)$ intersecting W^u. The point p_{out} is a solution to the 2PBVP defined by (4), (8) and (9) with $T = 0$. Figure 6(a)(a) illustrates an example of the set up for this homotopy step. The plane Σ^* is represented by a pink line, $E^s(p_{\text{out}}^t)$ is represented by a blue cross, and a curve representing S^t is sketched in neon green.

We increase T while allowing $\mathbf{u}_B(0)$ to decrease towards F_2. This step is illustrated in Figure 6(b) where an intermediate orbit is represented as a black curve with the fast segment indicated with double arrows and the slow segment indicated with a single arrow. The continuation is stopped at $\mathbf{u}(0)_B = B_{\text{in}} = 2.3 \times 10^{-1}$, just before it reaches $S1_B$. A sketch of the resulting orbit segment is shown in Figure 6(c).

The orbit segment illustrated in Figure 6(c) belongs to a two-parameter family of $\mathbf{u}$ that satisfy the boundary conditions (8) and (9). To select a one-parameter family of orbit segments from these, we impose the condition

$$\mathbf{u}(0) \in \Sigma^* \cap \left\{ \left(A\ B\ X\ Y \right) \in \mathbb{R}^4 \mid B = B_{\text{stop}} \right\} \tag{10}$$

that imposes three conditions on $\mathbf{u}(0)$ and is more restrictive than (8). The boundary condition (10) is represented as a yellow line in Figure 6(c). We define the three-dimensional space Ω spanned by the two stable eigenvectors of p_{out} and the vector parallel to the B- direction. Note that Ω is transverse to $E^u(C^t)$ and hence W^u. We impose the condition

$$\mathbf{u}(1) \in \Omega, \tag{11}$$

which imposes one condition on $\mathbf{u}(0)$ and is less restrictive than (9). Condition (9) is represented in Figure 6(c) as two navy blue intersecting planes. The integration time T is then increased forcing $\mathbf{u}(0)$ to approach $W^s \cap \Sigma^*$ and $\mathbf{u}(1)$ to approach $W^u \cap E^s(p_{\text{out}}^t)$. When a fold in T is reached $\mathbf{u}(0)$ and $\mathbf{u}(1)$ have intersected W^s and W^u, respectively and maximum integration time is attained.

The orbit segment that is obtained begins in Σ^* and has a fast approach to S^t before remaining $O(\varepsilon)$ close for an $O(1)$ time and so it lies on $W_{\Sigma^*}^s$. The final step is to continue the fold in T while allowing $u(0)_B$ to increase to obtain the rest of $W_{\Sigma^*}^s$.

Figure 4 shows two projections of $W_{\Sigma^*}^s(S^t)$. Although the manifold is two dimensional, it is necessary to visualise it in both the (B, A, X)- and (B, A, Y)- projections because it exists in four-dimensional space. Lying on $W_{\Sigma^*}^s(S^t)$ is a representative orbit segment, plotted in magenta. Plotted in black is the critical manifold. The view rotated relative to other figures to help illustrate the geometry of the slice. Orbits lying on $W_{\Sigma^*}^s(S^t)$ have a fast approach to S^t in X and Y before approaching mainly in the A-direction and then finally remaining close for an $O(1)$ amount of time.

In the case where we would like to compute W_{Σ}^s for a different Σ, given by constant values of A and Y (X), we must perform a second homotopy step after the first. Using the orbit segment represented in Figure 6(c) as a starting point, we impose (9) while keeping as free parameters T, $\mathbf{u}_B(0)$, $\mathbf{u}_X(0)$ $(\mathbf{u}_Y(0))$. In two runs, we continue $\mathbf{u}$ with each of the two coordinates that define Σ as our main continuation parameters. Once $\mathbf{u}(0) \in \Sigma$, we follow the rest of the procedure above while considering Σ instead of Σ^*.

Figure 6(d) illustrates a choice of Σ on the opposite side of the critical manifold from Σ^* in the (B, A)-projection. The orbit segment resulting from the second homotopy step is represented as a black curve. Conditions (10) and (11) are again illustrated with a yellow line and two intersecting navy blue planes, respectively.
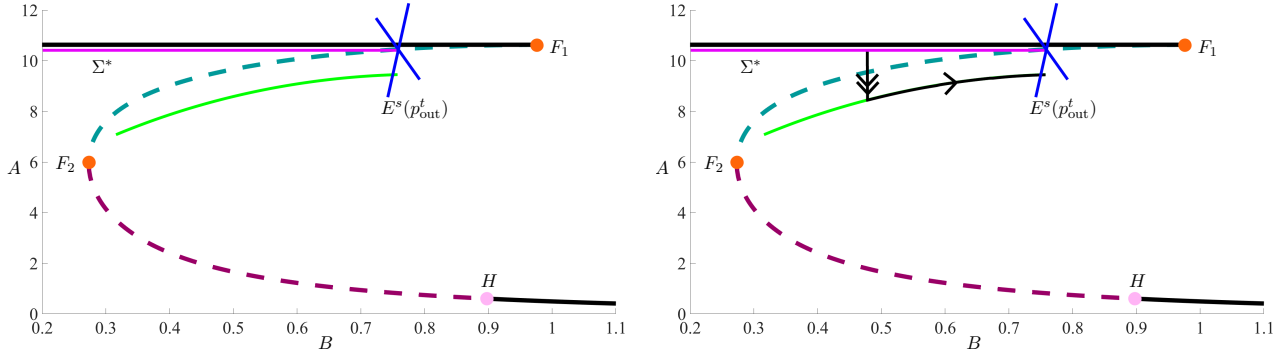
(a)A sketch of the first homotopy step in the algorithm for computing $W_{\Sigma^*}^s$. A projection of the plane Σ^* is represented as a pink line in the (B, A)-plane and labeled accordingly. The linear stable space, $E^s(p_{\text{out}}^t)$, is represented by a blue cross and is also labeled.

(b)An intermediate orbit in the first homotopy step is represented as a black curve. Fast segments are represented with double arrows while slow segments are represented with single arrows.
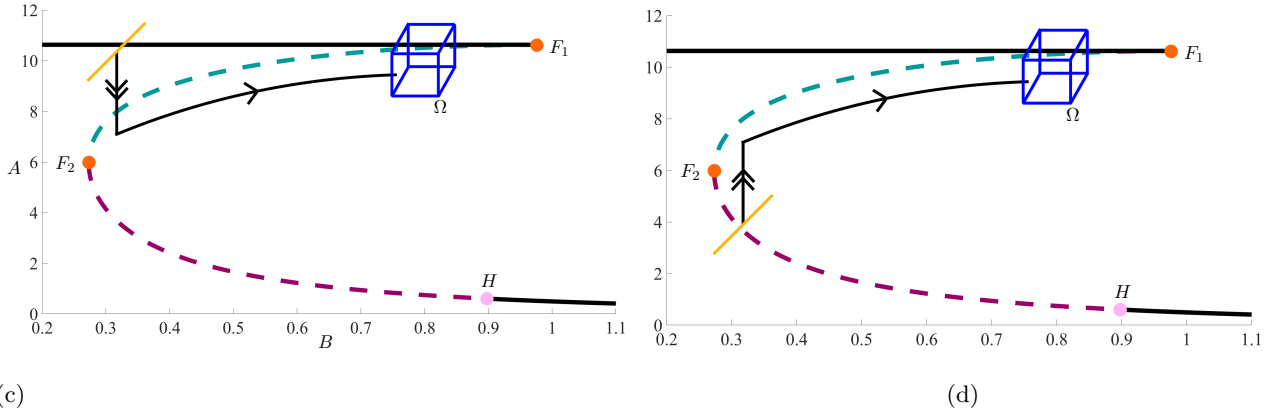
(c)

(d)

Fig. 3.   The slice $W_{\Sigma^*}^{\mathbf{s}}(S^t)$, represented in blue, projected into (B, A, X)-space (a) and (B, A, Y)-space (b) with a representative orbit segment plotted in magenta. Projections of the critical manifold are shown in black and the view is rotated relative to previous figures.

(a)

(b)

Fig. 4.   The slice $W_{\Sigma^*}^{\mathbf{s}}(S^t)$, represented in blue, projected into (B, A, X)-space (a) and (B, A, Y)-space (b) with a representative orbit segment plotted in magenta. Projections of the critical manifold are shown in black and the view is rotated relative to previous figures.
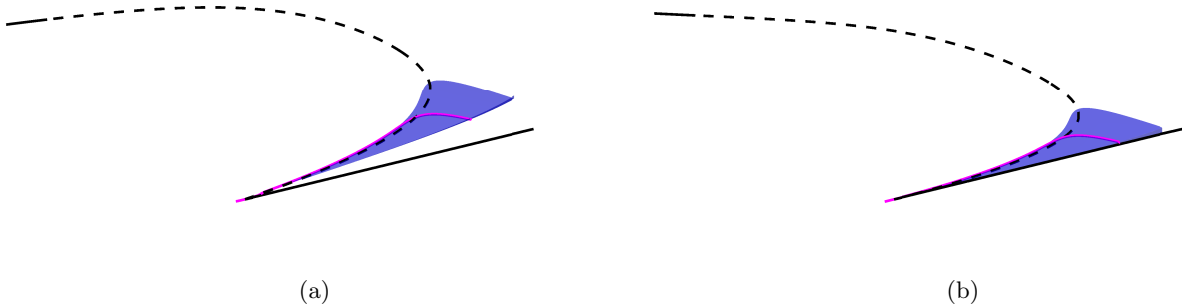
Figure 5 shows $W_{\Sigma^*}^s(S^t)$ and four slices W_{Σ}^s of $W^{\mathbf{s}}(S^t)$. Here Σ were selected as follows, $A \approx 10.6055$ and $Y \approx 2.3001 \times 10^{-4}$, $A = 2.0$ and $Y \approx 2.3001 \times 10^{-4}$, $A = 4.0$ and $X = 0.75$, $A = 4.0$ and $Y = 0.75$,
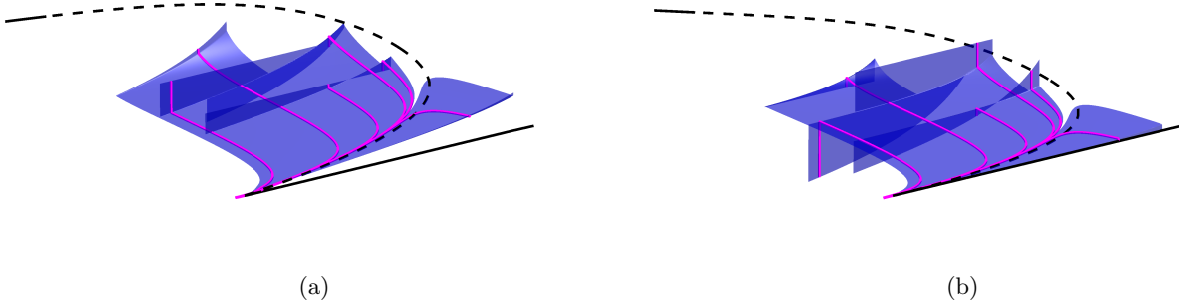
Fig. 5.   A variety of submanifolds of $W^{\mathbf{s}}(S^t)$, represented in blue, projected into (B, A, X)-space (a) and (B, A, Y)-space (b) with example orbit segments plotted in magenta. Projections of the critical manifold are shown in black and the view is rotated relative to previous figures.

$A = 6.0$ and $X = 0.5$. The slices W_{Σ}^s were defined as solutions to 4 with boundary conditions (8) (11) locally maximal T.

We note that, unlike the stable manifold of S^t computed in [Desroches *et al.*, 2009], each W_{Σ}^s in Figure 5 diverges backwards in time in the X- and Y- directions before reaching C^b. As it was an approximation of W^s, the stable manifold in the three-dimensional system suggests that there exists a W_{Σ}^s in the four-dimensional system that spirals around S^b in backward time for an appropriate choice of Σ. Such a surface would be the intersection of the two three-dimensional manifolds W^s and $W^u(S^b)$ would be a two-dimensional heteroclinic connection between C^t and C^b in the full four-dimensional system. A two-dimensional heteroclinic connection between two saddle slow manifolds of different type in a four-dimensional system would indeed be a novel phenomenon that does not occur in lower-dimensional systems.
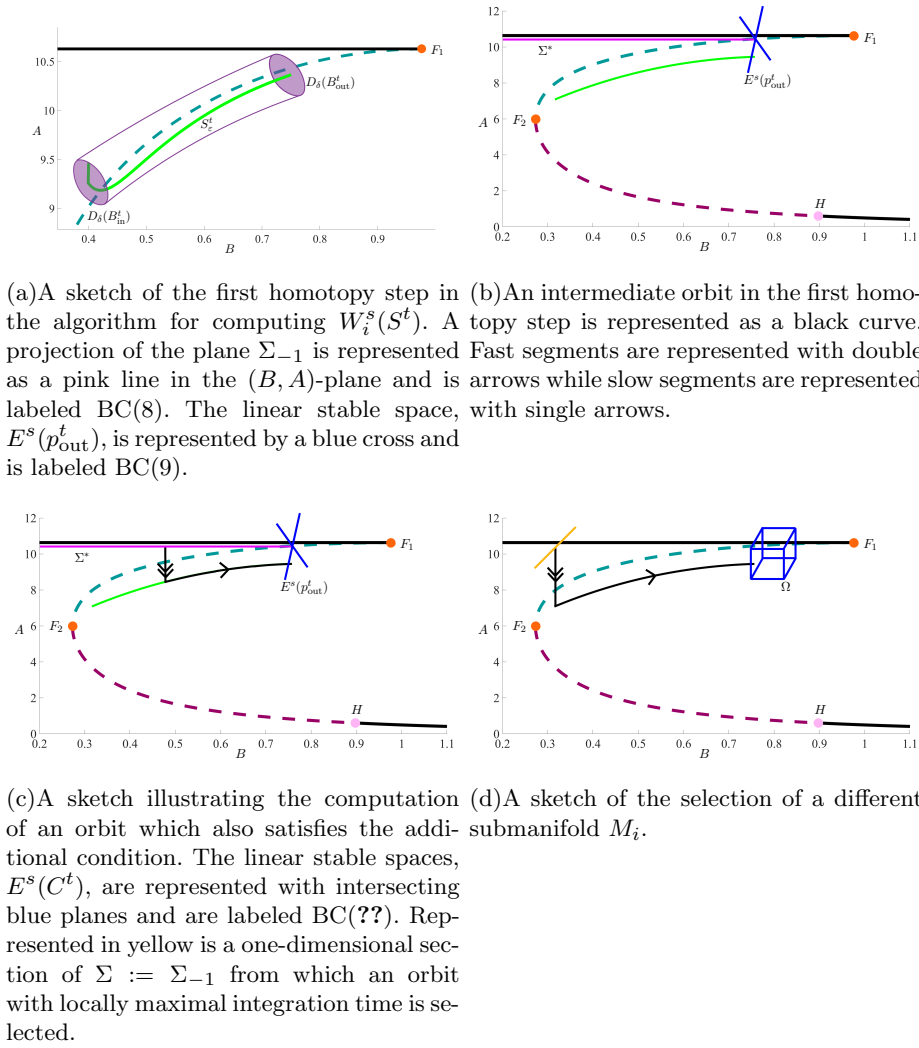
(a)A sketch of the first homotopy step in the algorithm for computing $W_i^s(S^t)$. A projection of the plane Σ_{-1} is represented as a pink line in the (B, A)-plane and is labeled BC(8). The linear stable space, $E^s(p_{\text{out}}^t)$, is represented by a blue cross and is labeled BC(9).

(b)An intermediate orbit in the first homotopy step is represented as a black curve. Fast segments are represented with double arrows while slow segments are represented with single arrows.

(c)A sketch illustrating the computation of an orbit which also satisfies the additional condition. The linear stable spaces, $E^s(C^t)$, are represented with intersecting blue planes and are labeled BC(**??**). Represented in yellow is a one-dimensional section of $\Sigma := \Sigma_{-1}$ from which an orbit with locally maximal integration time is selected.

(d)A sketch of the selection of a different submanifold M_i.

Fig. 6.   my caption

References

Benoît, E. [1982] "Systèmes lents-rapides dans $\mathbb{R}^3$ et leurs canards," *Proceedings of the Third Schnepfenried Geometry Conference* **2**, 159–191.

Benoît, E. [1985] "Enlacements de canards," *Comptes Rendus Mathematique Academie des Sciences* **300**, 225–230.

Benoît, E., Callot, J. F., Diener, F. & Diener, M. [1981] "Chasse au canard," *Collectanea Mathematica* **31**, 37–119.

Brøens, M. & Bar-Eli, K. [1991] "Canard explosion and excitation in a model of the belousov-zhabotinskii reaction," *Journal of Physical Chemistry A* **95**, 8706–8713.

Brøens, M., Krupa, M. & Wechselberger, M. [2006] "Mixed mode oscillations due to the generalized canard phenomenon," *Fields Institute Communications* , 39–63.

De Maesschalck, P. & Wechselberger, M. [2015] "Neural Excitability and Singular Bifurcations." *The Journal of Mathematical Neuroscience* **5**.

Desroches, M., Guckenheimer, J., Krauskopf, B., Kuehn, C., Osinga, H. & Wechselberger, M. [2012] "Mixed-Mode Oscillations with Multiple Time Scales." *SIAM Review* **54**, 211–288.

Desroches, M., Krauskopf, B. & Osinga, H. [2009] "The geometry of mixed-mode oscillations in the Olsen model for peroxidase-oxidase reaction." *Discrete & Continuous Dynamical Systems* **2**, 807–827.

Doedel, E. [2007] *AUTO-07p: Continuation and Bifurcation Software for Ordinary Differential Equations,*

URL http://indy.cs.concordia.ca/auto/, with major contributions from A.R. Champneys, F. Dercole, T.F. Fairgrieve, Y.A. Kuznetsov, R.C. Paffenroth, B. Sandstede, X. Wang and C. Zhang.

Farjami, S., Kirk, V. & Osinga, H. [2018] "Computing the Stable Manifold of a Saddle Slow Manifold." *SIAM Journal on Applied Dynamical Systems* **17**, 350–379.

Fenichel, N. [1979] "Geometric singular perturbation theory for ordinary differential equations," *Journal of Differential Equations* **31**, 53–98.

FitzHugh, R. [1955] "Mathematical models of threshold phenomena in the nerve membrane," *The bulletin of mathematical biophysics* **17**, 257–278.

Guckenheimer, J. [1985] "Singular hopf bifurcation in systems with two slow variables," *SIAM Journal on Applied Dynamical Systems* **7**, 1355–1377.

Hudson, J. L., Hart, M. & Marinko, D. [1979] "An experimental study of multiple peak periodic and nonperiodic oscillations in the belousov–zhabotinskii reaction," *The Journal of Chemical Physics* **71**, 1601–1606.

Krupa, M., Popović, N. & Kopell, N. [2008] "Mixed-mode oscillations in three time-scale systems: A prototypical example," *SIAM Journal on Applied Dynamical Systems* , 361–420.

Kuehn, C. & Szmolyan, P. [2015] "Multiscale Geometry of the Olsen Model and Non-classical Relaxation Oscillations." *Journal of Nonlinear Science* **25**, 583–629.

Olsen, L. [1983] "An enzyme reaction with a strange attractor." *Physics Letters A* **94**, 454–457.

Otto, C., Ludge, K., Vladimirov, A. G., Wolfrum, M. & Scholl, E. [2012] "Delay-induced dynamics and jitter reduction of passively mode-locked semiconductor lasers subject to optical feedback," *New Journal of Physics* **14**.

Piltz, S. H., Veerman, F., Maini, P. K. & Porter, M. A. [2017] "A predator–2 prey fast–slow dynamical system for rapid predator evolution," *SIAM Journal on Applied Dynamical Systems* **16**, 54–90.

van der Pol, B. [1927] "Forced oscillations in a circuit with non-linear resistance. (Reception with reactive triode)." *The London, Edinburgh, and Dublin Philosophical Magazine and Journal of Science* **3**, 65–80.